MOLECULAR PLANT PATHOLOGY (2018) 19(3), 731–743 DOI: 10.1111/mpp.12558

The 50 distal amino acids of the 2A^{HP} homing protein of *Grapevine fanleaf virus* elicit a hypersensitive reaction on *Nicotiana occidentalis*

ISABELLE R. MARTIN[1], EMMANUELLE VIGNE[1], FRANÇOIS BERTHOLD[2]†, VÉRONIQUE KOMAR[1], OLIVIER LEMAIRE[1], MARC FUCHS[3] AND CORINNE SCHMITT-KEICHINGER[2,*]

[1]*Université de Strasbourg, INRA, SVQV UMR-A 1131, Colmar 68000, France*

[2]*Université de Strasbourg, CNRS, IBMP UPR 2357, Strasbourg 67000, France*

[3]*Department of Plant Pathology and Plant–Microbe Biology, Cornell University, New York State Agricultural Experiment Station, Geneva, NY 14456, USA*

SUMMARY

Avirulence factors are critical for the arm's race between a virus and its host in determining incompatible reactions. The response of plants to viruses from the genus *Nepovirus* in the family *Secoviridae*, including *Grapevine fanleaf virus* (GFLV), is well characterized, although the nature and characteristics of the viral avirulence factor remain elusive. By using infectious clones of GFLV strains F13 and GHu in a reverse genetics approach with wild-type, assortant and chimeric viruses, the determinant of necrotic lesions caused by GFLV-F13 on inoculated leaves of *Nicotiana occidentalis* was mapped to the RNA2-encoded protein 2A^{HP}, particularly to its 50 C-terminal amino acids. The necrotic response showed hallmark characteristics of a genuine hypersensitive reaction, such as the accumulation of phytoalexins, reactive oxygen species, pathogenesis-related protein 1c and hypersensitivity-related (hsr) 203J transcripts. Transient expression of the GFLV-F13 protein 2A^{HP} fused to an enhanced green fluorescent protein (EGFP) tag in *N. occidentalis* by agroinfiltration was sufficient to elicit a hypersensitive reaction. In addition, the GFLV-F13 avirulence factor, when introduced in GFLV-GHu, which causes a compatible reaction on *N. occidentalis*, elicited necrosis and partially restricted the virus. This is the first identification of a nepovirus avirulence factor that is responsible for a hypersensitive reaction in both the context of virus infection and transient expression.

Keywords: avirulence factor, defence, hypersensitive reaction, *Nepovirus*, reverse genetics, *Secoviridae*, symptom determinant.

INTRODUCTION

The infection of a plant by a virus can result in a compatible reaction, which often leads to systemic symptoms, or in an incompatible reaction, as a result of the recognition of an avirulence (Avr) factor of the pathogen by a resistance gene of the host plant, which causes a hypersensitive reaction (HR). The two types of plant–virus interaction are well exemplified by the tobacco–*Tobacco mosaic virus* (TMV) interaction (Scholthof, 2008). In tobacco cultivars devoid of the *N* gene from *Nicotiana glutinosa*, the interaction is compatible with TMV, usually causing chlorotic local lesions, followed by systemic mosaic symptoms. In contrast, in tobacco cultivars containing the *N* gene, the interaction is incompatible with TMV, producing local necrotic lesions in which the virus remains localized in a few hundred cells around the entry site, no systemic virus spread occurs and apical leaves remain symptomless. Localized symptoms primarily result from an HR (Scholthof, 2008).

HR typically activates a non-specific plant response, including a kinase cascade, a burst of reactive oxygen species (ROS), such as hydrogen peroxide (H_2O_2), an increase in Ca^{2+} and salicylic acid content, an accumulation of antimicrobial compounds, such as phytoalexins, and an overexpression of defence gene products, such as pathogenesis-related (PR) proteins (Dangl and Jones, 2001; Künstler *et al.*, 2016; de Ronde *et al.*, 2014). The resulting cell death generally contributes to resistance by limiting the propagation of the virus (Bendahmane *et al.*, 1999; Dinesh-Kumar *et al.*, 2000; Künstler *et al.*, 2016; de Ronde *et al.*, 2014). Resistance can be extreme when the virus is localized to the infection site or non-existent when the virus induces necrosis in the whole plant as a result of a systemic HR. The timing and speed of the host response to virus infection are predicted to determine the varying degrees of resistance and symptoms seen at the macroscopic level (Künstler *et al.*, 2016).

Nepoviruses cause diseases in fruit, vegetable and ornamental crops, and infect herbaceous hosts, on which they induce a range of symptoms, depending on both the host–virus combination and environmental conditions (Fuchs *et al.*, 2017; Sanfaçon, 2008). On *Nicotiana* spp., nepoviruses often cause symptoms on inoculated

* *Correspondence:* Email: keichinger@unistra.fr

† *Present address*: Université de Strasbourg, INRA, SVQV UMR-A 1131, Colmar 68000, France

Sequence of *N. occidentalis hsr203J* gene fragment was deposited in GenBank and given accession number KY363392.

leaves and a few uninoculated apical leaves, whilst the following emerging leaves remain asymptomatic. This phenomenon, known as recovery, is associated with RNA silencing (Ghoshal and Sanfaçon, 2015; Palukaitis, 2011). In addition to the recovery phenotype, *Tomato ringspot virus* (ToRSV) induces a systemic HR-like response on *N. benthamiana* (Jovel *et al.*, 2007), whereas systemic spread of ToRSV is much more limited in tobacco plants (Jovel *et al.*, 2011). Although the dependence of HR on salicylic acid and temperature has been demonstrated for ToRSV, the viral effector of HR remains elusive.

Grapevine fanleaf virus (GFLV) is another species of the genus *Nepovirus* in the family *Secoviridae*. It is the major causal agent of grapevine degeneration disease (Andret-Link *et al.*, 2004). Its genome is composed of two single-stranded, positive-sense RNAs that are covalently linked to a small viral protein (VPg) at their 5′ end and contain a polyA tail at their 3′ extremity. Each genomic RNA encodes a single polyprotein, which is proteolytically cleaved by the viral proteinase ($1D^{Pro}$) into functional proteins. RNA1 encodes proteins involved in virus replication and polyprotein processing, whereas RNA2 encodes proteins involved in virus movement ($2B^{MP}$) and morphogenesis ($2C^{CP}$) in addition to RNA2 replication ($2A^{HP}$) (Andret-Link *et al.*, 2004; Fuchs *et al.*, 2017; Gaire *et al.*, 1999). Systemic GFLV infection of plants requires both genomic RNAs (Viry *et al.*, 1993).

Preliminary work has revealed a differential reaction of GFLV strains GHu and F13 on *N. occidentalis*. Whereas GFLV-GHu induces systemic vein clearing and mosaic symptoms in uninoculated apical leaves, indicative of a compatible reaction, strain F13 causes chlorotic to necrotic lesions on inoculated leaves and produces variable phenotypes on uninoculated apical leaves, ranging from a lack of symptoms to a few chlorotic or necrotic spots. The response of GFLV-F13 on *N. occidentalis* is suggestive of an HR. Here, we expand on these initial observations and characterize the HR. Our research reveals that GFLV-F13 carries an Avr function that maps to the last 50 amino acids of protein $2A^{HP}$ and partially limits the virus to inoculated leaves. This is the first identification and characterization of a nepovirus Avr factor that limits virus spread.

RESULTS

GFLV-F13 induces necrosis on *N. occidentalis*, whereas GFLV-GHu causes mosaic symptoms

Wild-type (WT) GFLV strains F13 and GHu (Vigne *et al.*, 2013) induced different reactions on *N. occidentalis* when inoculated at 350 ng/plant. GFLV-F13 caused small chlorotic and/or necrotic lesions on inoculated leaves at 3–5 days post-inoculation (dpi) (Fig. 1c). Necrotic lesions generally expanded and coalesced at 10 dpi (Fig. 1b). In addition, systemic infection rates were moderate (70%), as shown by double antibody sandwich-enzyme-linked immunosorbent assay (DAS-ELISA) on uninoculated apical leaves, with symptoms falling into two categories: symptomless leaves (Table 1 and Fig. 1e) and leaves with chlorotic to necrotic spots with poorly defined borders and some distortions (Table 1 and Fig. 1f). In contrast, GFLV-GHu consistently remained asymptomatic on inoculated leaves (Fig. 1a) and caused a systemic infection, as judged from the vein clearing followed by mosaic symptoms on uninoculated apical leaves at 7–8 dpi (Fig. 1a,d). These symptoms vanished at 12–14 dpi in a process very similar to that described previously on *N. benthamiana* (Vigne *et al.*, 2013).

To characterize the reaction of the two GFLV strains on *N. occidentalis*, the virus titre was estimated in inoculated and uninoculated leaves by semi-quantitative DAS-ELISA. Systemic infection by GFLV-GHu resulted in a high virus titre (50 μg of virus per gram of fresh tissue on average) in both inoculated and uninoculated leaves (Table 1). In contrast, the titre of GFLV-F13 was very low (below 5 μg/g of fresh tissue on average) in symptomatic apical leaves, whereas symptomless leaves remained free of virus (Table 1). These results show that the GFLV-GHu–*N. occidentalis* interaction is compatible, whereas GFLV-F13, although inducing variable phenotypes on uninoculated apical leaves, consistently causes necrosis on inoculated leaves and accumulates at very low levels.

Viral determinants of the necrotic phenotype map to the GFLV-F13 $2A^{HP}$ coding sequence

In order to identify the viral determinants of the necrotic phenotype caused by GFLV-F13 on *N. occidentalis*, transcripts derived from infectious clones of GFLV-F13 (Viry *et al.*, 1993) and GFLV-GHu (Vigne *et al.*, 2013) were used in inoculation experiments. As expected, G1G2 [transcripts derived from cDNA clones of GFLV-GHu RNA1 and RNA2 in pG1 and pG2, respectively (Vigne *et al.*, 2013)] reproduced the compatible infection observed with the parental WT GFLV-GHu in terms of symptoms (absence on inoculated leaves and mosaic on apical leaves) and high virus titre (Table 1). F1F2 [transcripts derived from cDNA clones of GFLV-F13 RNA1 and RNA2 in pF1 and pF2, respectively (Vigne *et al.*, 2013)] induced a necrotic reaction on inoculated leaves. However, the necrosis was less severe than with the parental WT GFLV-F13, although the virus titre was comparably low. All uninoculated leaves of plants infected with F1F2 remained symptomless and virus free (Table 1). In spite of the slight differences in behaviour of F1F2 and WT GFLV-F13, assortants of the synthetic inocula F1F2 and G1G2 were further used to map the viral determinant(s) responsible for necrosis on *N. occidentalis*.

N. occidentalis inoculated with assortant G1F2 exhibited necrotic lesions on inoculated leaves and either no symptoms or chlorotic or necrotic spots with leaf distortion on uninoculated apical leaves, whereas assortant F1G2 caused mosaic symptoms on uninoculated apical leaves and inoculated leaves remained

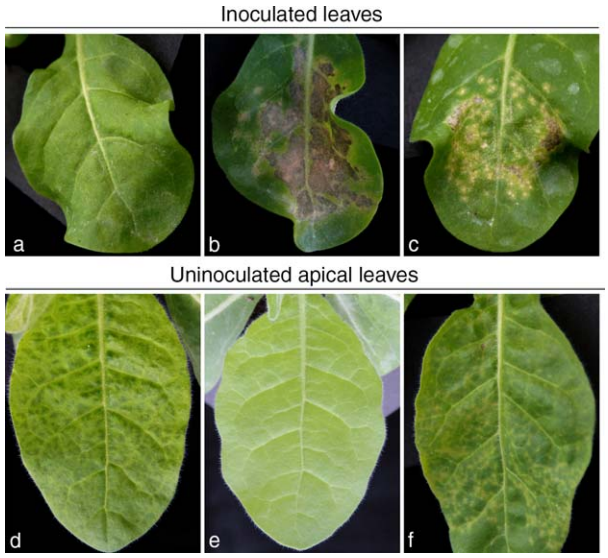

Fig. 1 Types of symptom induced by wild-type, synthetic, assortant and chimeric *Grapevine fanleaf virus* (GFLV) strains on inoculated (a–c) and uninoculated apical (d–f) leaves of *N. occidentalis* at 8 days post-inoculation (dpi). (a) Asymptomatic leaf (as exemplified here with a G1G2-inoculated leaf). (b) Intense necrotic lesions (NL) (here photographed on a G1G2($2A_F$)-inoculated leaf). (c) Necrotic lesions (NL) (as observed on an F1F2-inoculated leaf). (d) Mosaic symptoms (here photographed on an uninoculated leaf of a G1G2-inoculated plant). (e) Asymptomatic apical leaf (here photographed on an F1F2-inoculated plant). (f) Intense chlorotic to necrotic spots with some leaf distortion (CNS to LD) [here photographed on a plant inoculated with the recombinant G1G2($2A_F$)]. (See also Table 1.)

asymptomatic (Table 1). A high virus titre (70 and 40 μg/g in inoculated and apical leaves, respectively) for F1G2 and a low virus titre (2.5 and 3 μg/g in inoculated and apical leaves, respectively) for G1F2 were determined (Table 1). These results demonstrate the involvement of GFLV-F13 RNA2 in the necrotic phenotype.

To further identify the sequence responsible for the necrotic reaction of GFLV-F13 on *N. occidentalis*, the RNA2-encoded $2A^{HP}$ coding sequence was exchanged between strains F13 and GHu to develop chimeric constructs. Recombinant F1F2($2A_G$) with the $2A^{HP}$ coding sequence of GHu in the F13 RNA2 caused a compatible reaction with no symptoms on inoculated leaves, mosaic symptoms on apical leaves and a high virus titre (40 and 70 μg/g of fresh tissue in inoculated and apical leaves, respectively; Table 1). In contrast, recombinant G1G2($2A_F$) with the $2A^{HP}$ coding sequence of F13 in the GHu RNA2 caused intense necrotic lesions on inoculated leaves and the virus titre was low (Table 1). On sequencing the progeny of recombinants F1F2($2A_G$) and G1G2($2A_F$) within the 5′ untranslated region (UTR), the complete $2A^{HP}$ coding region and the beginning of the $2B^{MP}$ coding region after immunocapture-reverse transcription-polymerase chain reaction (IC-RT-PCR) indicated genetic stability and consistency with the sequence of the inoculum. Thus, the GFLV-F13 RNA2-encoded $2A^{HP}$ region determines the necrotic phenotype on inoculated leaves of *N. occidentalis*.

The necrotic phenotype of GFLV-F13 on *N. occidentalis* displays hallmark characteristics of an HR

N. occidentalis inoculated with WT GFLV-F13, assortants and recombinants harbouring the $2A^{HP}$ sequence of F13 exhibited necrotic lesions on inoculated leaves (Fig. 1 and Table 1), accumulated 7–10 times less virus than GFLV inocula devoid of the F13 $2A^{HP}$ coding sequence and showed variable symptom severity on uninoculated apical leaves, ranging from no symptoms to intense necrotic spots, all reminiscent of an HR. To verify the occurrence of an HR, inoculated leaves of *N. occidentalis* were tested for hallmarks of HR, such as the accumulation of phytoalexins, ROS, PR proteins and hypersensitivity-related (hsr) 203J transcripts.

N. occidentalis leaves inoculated with WT GFLV-F13, synthetic F1F2 or chimeric G1G2($2A_F$), observed under UV illumination, showed bright blue rings of fluorescent cells around necrotic lesions as early as 2 dpi, demonstrating an increase in scopoletin and scopolin content (Chong *et al.*, 2002) of the living cells surrounding the necrotic lesions (Fig. 2a). In contrast, *N. occidentalis* leaves inoculated with WT GFLV-GHu, synthetic G1G2 or chimeric F1F2($2A_G$) only showed the red fluorescence background of chlorophyll (Fig. 2a). No increase in scopoletin was observed.

The massive production of ROS, known as the oxidative burst, is an early response activated in many incompatible interactions (Lamb and Dixon, 1997). This oxidative burst can easily be visualized *in situ* through the instant polymerization of 3,3′-diaminobenzidine (DAB) when it comes into contact with H_2O_2 in the presence of peroxidases (Thordal-Christensen *et al.*, 1997). The application of DAB to the inoculated leaves of *N. occidentalis* showed that only GFLV constructs harbouring the F13 $2A^{HP}$ sequence, i.e. WT F13, synthetic F1F2 and chimeric G1G2($2A_F$), presented brown speckles, indicating H_2O_2 accumulation (Fig. 2b). A close observation of leaf discs with a binocular microscope confirmed the spatial correlation between necrotic spots and H_2O_2 accumulation in surrounding living cells (data not shown). Leaves inoculated with the synthetic G1G2 and chimeric F1F2($2A_G$) constructs remained unstained and similar to mock-inoculated leaf discs (Fig. 2b).

The PR1c protein, a defence-related inducible protein (Cornelissen *et al.*, 1986; Sels *et al.*, 2008), accumulated to detectable levels in *N. occidentalis* leaves inoculated with the necrogenic synthetic F1F2 and recombinant G1G2($2A_F$), but not in leaves infected with synthetic G1G2 and recombinant F1F2($2A_G$), which do not induce symptoms on inoculated leaves (Fig. 2c).

To further characterize the necrotic response of *N. occidentalis* inoculated with F1F2 and G1G2($2A_F$), the accumulation level of hsr203J transcripts, which are correlated with controlled cell death in *Solanaceae* plants as diverse as tobacco and tomato (Pontier

Table 1 Symptoms and virus titres of wild-type, synthetic, assortant and chimeric *Grapevine fanleaf virus* (GFLV) strains in inoculated and apical leaves of *Nicotiana occidentalis*.

				Symptoms on leaves§		Virus titre¶ (μg of virus/g of fresh leaf tissue)			
Inoculum*		Exp†	Ratio‡	Inoculated	Apical	Inoculated		Apical	
Wild-type	GHu	1	10/10	–	Mosaic	51.1	(±6.1)	45.0	(±7.2)
	F13	1	3/10	NL	–	1.7	(±0.5)	0	(±0.0)
			7/10	NL	CNS to LD	2.3	(±0.6)	3.0	(±2.9)
Synthetic	G1G2	1	10/10	–	Mosaic	61.5	(±6.2)	54.1	(±8.9)
	G1G2	2	10/10	–	Mosaic	50.0	(±6.4)	51.5	(±9.8)
	F1F2	1	10/10	NL	–	1.9	(±0.4)	0	(±0.0)
	F1F2	2	10/10	NL	–	1.2	(±0.4)	0	(±0.0)
Assortant	F1G2	1	10/10	–	Mosaic	74.4	(±11.3)	39.3	(±9.8)
	G1F2	1	3/10	NL	–	2.4	(±0.5)	0	(±0.0)
			6/10	NL	CNS to LD	2.6	(±0.5)	6.7	(±12.7)
Chimeric	F1F2($2A_G$)	2	10/10	–	Mosaic	40.0	(±4.1)	68.9	(±10.5)
	G1G2($2A_F$)	2	10/10	NL	CNS to LD	1.3	(±0.5)	10.3	(±6.7)
	F1F2($2A_{F209G}$)	2	10/10	–	Mosaic	41.1	(±9.1)	97.6	(±9.5)
	G1G2($2A_{G209F}$)	2	1/10	NL	–	0.6		0	
			9/10	NL	CNS to LD	0.8	(±0.4)	23.9	(±20.3)

*Crude sap of *Chenopodium quinoa* plants infected with wild-type, synthetic, assortant or chimeric GFLV strains was used as inoculum at 350 ng/plant.

†Two independent experiments performed on 18 January (Exp 1) and 1 February (Exp 2) 2016 on 10 plants each. The GFLV assortants G1G2 and F1F2 were used in both experiments.

‡Number of plants showing a given phenotype divided by the total number of inoculated plants.

§Necrotic lesions (NL) or chlorotic and necrotic spots (CNS) to leaf deformation (LD).

¶Virus concentration ± standard deviation (in parentheses) estimated by semi-quantitative double antibody sandwich-enzyme-linked immunosorbent assay (DAS-ELISA).

et al., 1994, 1998), was evaluated. As no *hsr203J* sequence was available in public databases for *N. occidentalis* at the onset of this study, primers were designed on the basis of *hsr203J* of *N. tabacum* (GenBank X77136). A unique cDNA fragment of 391 bp was amplified by RT-PCR from total RNA extracts of *N. occidentalis* (GenBank KY363392), which shared 93.9% nucleotide identity with the corresponding fragment of the *N. tabacum hsr203J* gene. From this sequence, new primers were designed for quantitative RT-PCR analysis of the steady-state level of hsr203J transcripts in infected *N. occidentalis*. The results indicated a four-fold increased accumulation of hsr203J transcripts in necrotic leaves inoculated with synthetic F1F2 and recombinant G1G2($2A_F$), compared with symptomless leaves inoculated with synthetic G1G2 and recombinant F1F2($2A_G$) (Fig. 2d).

Knowing that enhanced production of phytoalexins, ROS, PR proteins and hsr203J transcripts is associated with HR (Watanabe and Lam, 2006), we can conclude that the necrotic phenotype of GFLV constructs carrying an F13-$2A^{HP}$ coding sequence on *N. occidentalis* corresponds to an HR.

Protein $2A^{HP}$ of GFLV-F13 elicits HR in *N. occidentalis*

To characterize the viral elicitor of the necrotic response of GFLV-F13 on *N. occidentalis*, an enhanced green fluorescent protein (EGFP)-tagged $2A^{HP}$ protein and a mutant $2A^{HP}$ construct bearing a stop codon downstream of the start codon (construct $2A_{F\text{-}Stop}$:EGFP) were used in a transient expression system (Fig. 3a). None of the constructs caused necrosis on *N. benthamiana* plants, ruling out their possible phytotoxicity *in planta*. No fluorescent protein was observed in *N. occidentalis* and *N. benthamiana* by confocal microscopy observations following agroinfiltration of bacteria containing the $2A_{F\text{-}Stop}$:EGFP construct, although the production of the corresponding transcript was readily detected by RT-PCR (Fig. 3b). In contrast, EGFP, $2A_F$:EGFP and $2A_G$:EGFP proteins were visible at 2 dpi. In addition, EGFP had a typical nucleocytoplasmic localization, as anticipated, whereas $2A_F$:EGFP and $2A_G$:EGFP formed punctate structures in the cytoplasm (Fig. 3c). This subcellular localization is in agreement with the localization of $2A_F$:GFP in protoplasts either early during infection or in the absence of virus (Gaire *et al.*, 1999). Following the agroinfiltration of *N. occidentalis* leaves, only $2A_F$:EGFP induced chlorosis at 3 dpi in the infiltrated leaf area; this symptom evolved into necrosis at 5–7 dpi. By contrast, no symptoms were visible in leaf patches of *N. occidentalis* infiltrated with agrobacteria carrying $2A_{F\text{-}Stop}$:EGFP, EGFP or $2A_G$:EGFP constructs (Fig. 3d). The observation of agroinfiltrated leaf areas under UV light further showed that scopolin and scopoletin production was correlated with the expression of only $2A_F$:EGFP (Fig. 3e). These observations demonstrate that the GFLV-F13 $2A^{HP}$ protein, rather than its coding RNA sequence, induces necrosis on *N. occidentalis*.

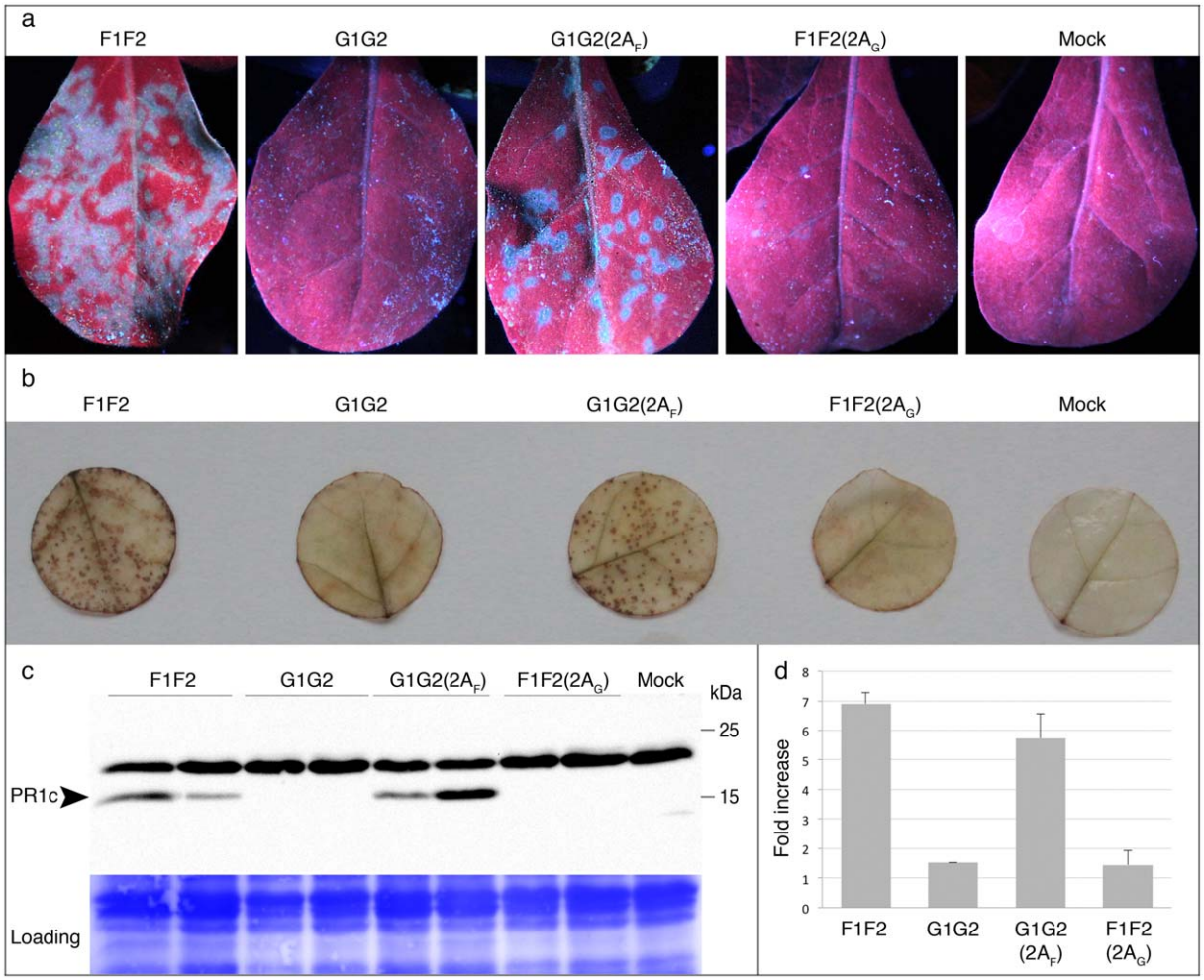

Fig. 2 Induction of hypersensitive reaction (HR) markers by synthetic, assortant and chimeric *Grapevine fanleaf virus* (GFLV) strains on inoculated leaves of *Nicotiana occidentalis*. (a) Leaves infected with F1F2 and G1G2(2A$_F$) photographed under UV (354 nm) light show a fluorescent blue halo of phytoalexin-producing cells around the necrotic lesions. (b) 3,3′-Diaminobenzidine (DAB) staining of hydrogen peroxide production in leaf discs infected with F1F2 and G1G2(2A$_F$) at 3 days post-inoculation (dpi). (c) Western blot analysis of pathogenesis-related 1c (PR1c) protein accumulation at 10 dpi. Total protein samples of two separate plants are shown for each construct. (d) Relative accumulation of hypersensitivity-related (hsr) 203J transcripts as determined by quantitative reverse transcription-polymerase chain reaction (RT-PCR) compared with mock-inoculated plants using EF1α transcripts as a reference (mock inoculation consisted here in rubbing the leaves with grinding buffer).

Transient expression of 2A$_F$:EGFP induced the accumulation of HR markers, such as H_2O_2, PR1c (although weaker than in the viral context) and hsr203J transcripts, in agroinfiltrated leaf patches of *N. occidentalis* (Fig. 3f–h). These observations previously made for necrogenic synthetic F1F2 and recombinant G1G2(2A$_F$) confirmed that GFLV-F13 protein $2A^{HP}$ is the viral elicitor of the necrotic phenotype on *N. occidentalis*.

The C-terminal 50 amino acids of GFLV-F13 $2A^{HP}$ determine HR

Protein $2A^{HP}$ of GFLV strains F13 and GHu (Fig. 4a) contain 258 amino acids, 170 (residues 89–258) of which are included in the NeA_P2 motif (pfam12312), a signature motif shared by P2 polyproteins of subgroup A nepoviruses that also encompass the $2B^{MP}$ and $2C^{CP}$ coding sequences. The 88 residues upstream of this motif constitute the N-terminal region of protein $2A^{HP}$. Sequence analysis with myHits (http://myhits.isb-sib.ch) highlighted the existence of two regions particularly rich in proline (Pro) residues, both including a four to five Pro stretch. These regions were designated PRM1 for Proline Rich Motif-1 (amino acids 86–118) and PRM2 (amino acids 199–214). The highest divergence (34%) between the F13 and GHu protein $2A^{HP}$ sequence is in the C-terminal region downstream of the second PRM (amino acids 215–258). Interspecies recombination between GFLV and *Arabis mosaic virus* (ArMV) at the origin of the mosaic structure in the

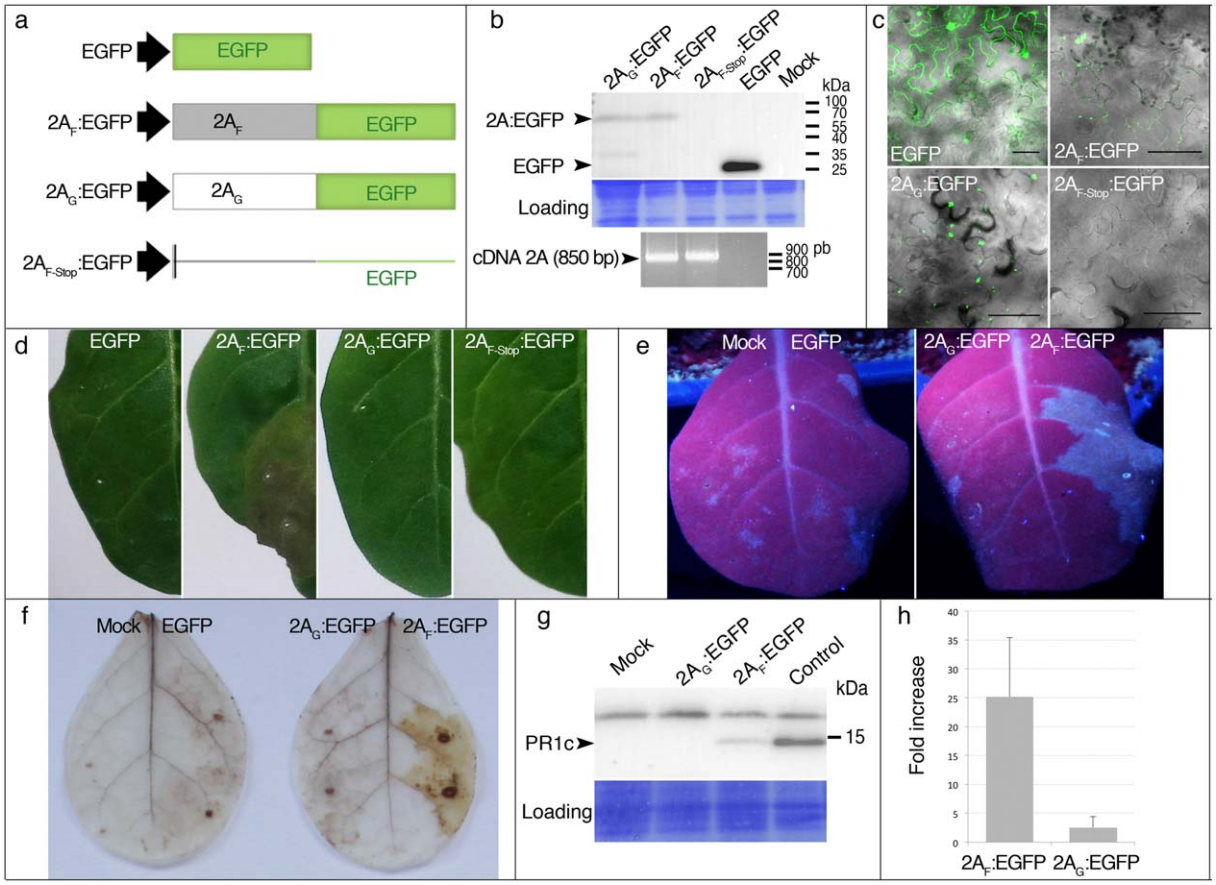

Fig. 3 Protein 2A^{HP} of GFLV strain F13 elicits necrosis on *Nicotiana occidentalis*. (a) Constructs used to transiently express protein 2A^{HP} of GFLV in fusion with EGFP or its coding RNA. Black arrows represent the 35S promoter, horizontal lines represent untranslatable sequences and the vertical line represents the mutated initiation and stop codons. (b) Expression of the GFLV 2A^{HP} EGFP-tagged constructs was verified by western blot using anti-GFP antibodies and/or by reverse transcription-polymerase chain reaction (RT-PCR) using 2A^{HP}-specific primers. (c) Proteins 2A$_F$:EGFP and 2A$_G$:EGFP form cytoplasmic aggregates, whereas EGFP shows a nucleocytoplasmic localization. No fluorescence is detected with the 2A$_{F\text{-}Stop}$:EGFP construct. Scale bar, 50 μm. Confocal images show the superimposition of fluorescence and differential interference contrast (DIC) channels in *N. benthamiana*. (d–h) Agroinfiltrated patches of *N. occidentalis*. (d) Patches photographed at 5 dpi under visible light. (e) Phytoalexin production photographed at 3 dpi under UV light. Detection of H_2O_2 DAB staining (f), pathogenesis-related 1c (PR1c) by western blot (g) and hypersensitivity-related (hsr) 203J transcripts by quantitative RT-PCR (h). The mock sample was infiltrated with agroinfiltration buffer only. Fold increase indicates expression compared with plant patches expressing unfused EGFP.

C-terminus of GFLV-GHu protein 2A^{HP} accounts for this high divergence in the C-terminal part of the protein (Vigne *et al.*, 2008), rather than in its N-terminal region, which shows only 4.5% divergence.

Because sequence alignments were not very useful at informing the domain of protein 2A^{HP} responsible for the necrotic phenotype on *N. occidentalis*, a series of deletion mutants was constructed for transient expression assays (Fig. 4a). When expressed as fusion products to EGFP in *N. occidentalis* leaves, the mutant proteins, ΔN46, ΔN82, ΔPRM1 and ΔM75, elicited a necrotic patch at 5–7 dpi and a blue halo was observed under UV illumination at 2 or 3 dpi, similar to the WT control (Fig. 4b). No necrosis was observed with protein ΔC43, in which the 43 C-terminal residues are deleted, whereas necrosis was very weak with protein ΔPRM2, in which the second PRM is deleted. In addition, the blue halo under UV illumination was weaker for these two mutants. The drastic reduction in the response of *N. occidentalis* infiltrated with mutant proteins with deletion of the 58 C-terminal residues suggests the involvement of the protein 2A^{HP} C-terminus in the HR. However, large deletions can cause changes in protein stability, conformation or localization, revealing an indirect involvement of the deleted region rather than a direct and active effect. This possibility was suggested for some deletion 2A^{HP} mutants by their altered subcellular localization (Fig. 4b). Thus, to confirm the role of the C-terminus of GFLV-F13 protein 2A^{HP} in the necrotic response of *N. occidentalis*, the

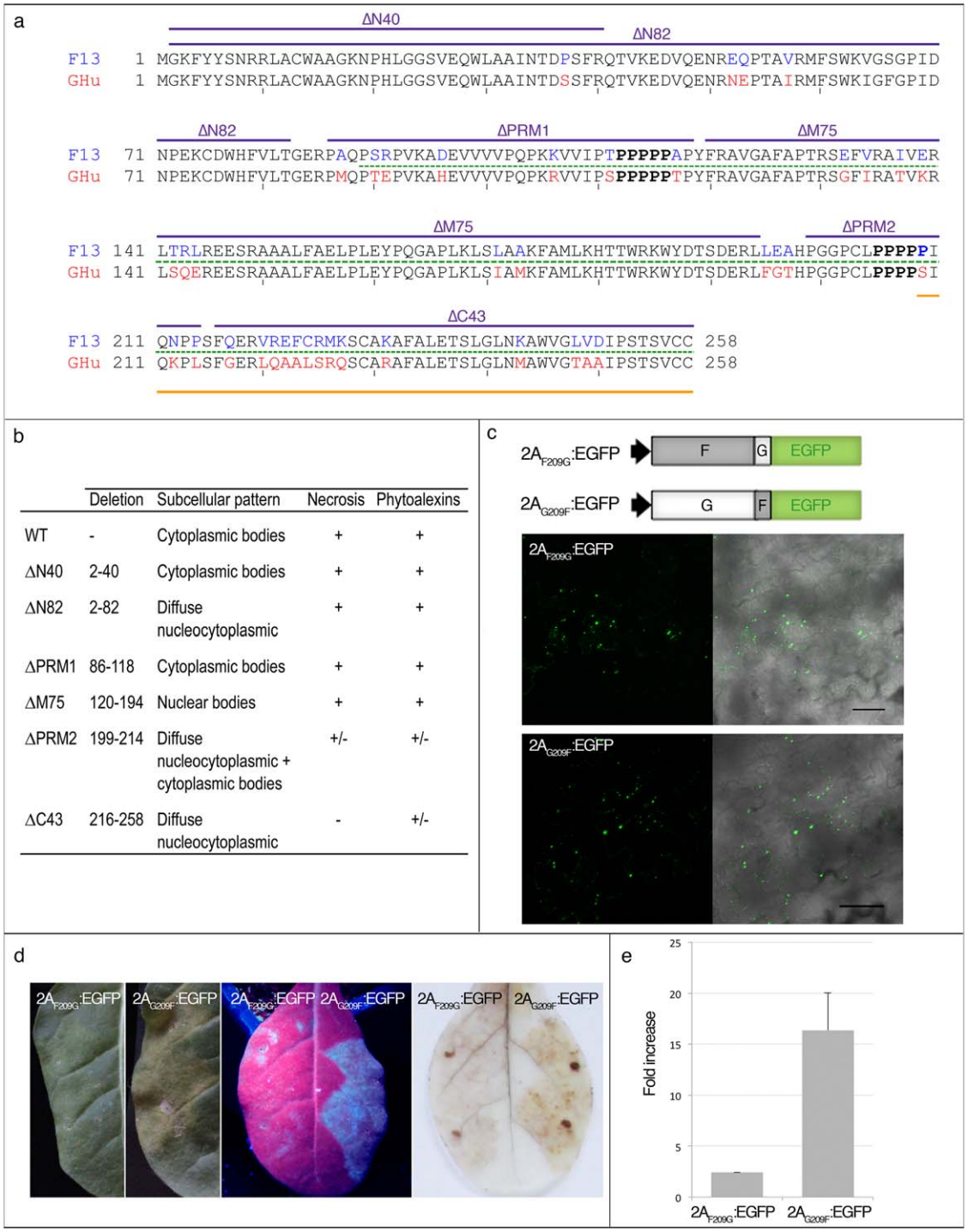

	Deletion	Subcellular pattern	Necrosis	Phytoalexins
WT	-	Cytoplasmic bodies	+	+
ΔN40	2-40	Cytoplasmic bodies	+	+
ΔN82	2-82	Diffuse nucleocytoplasmic	+	+
ΔPRM1	86-118	Cytoplasmic bodies	+	+
ΔM75	120-194	Nuclear bodies	+	+
ΔPRM2	199-214	Diffuse nucleocytoplasmic + cytoplasmic bodies	+/-	+/-
ΔC43	216-258	Diffuse nucleocytoplasmic	-	+/-

Fig. 4 The 50 C-terminal residues of protein 2A^{HP} of GFLV strain F13 elicit HR. a. Sequence alignment of proteins 2A$_F$ and 2A$_G$. Common residues are in black and divergent residues are in blue (F13) and red (GHu). The proline residues conserved among nepoviruses are in bold. The green dotted line represents the sequence of the NeA_P2 conserved domain. The purple lines delineate deleted residues in the 2A$_F$ mutants. The orange line underlines the 50 residues selected for reciprocal exchange. b. Subcellular localization and phenotype of protein 2A^{HP} mutants when transiently expressed in *N. occidentalis* leaves as a fusion to EGFP. c. Schematic representation of the two recombinant 2A^{HP} constructs with the swapped residues and their expression in *N. occidentalis* observed by confocal microscopy. Scale bar: 50 μm. Protein 2A^{HP} containing the fifty distal residues of GFLV-F13 induced necrotic symptoms (d, second left panel), the production of phytoalexins visualized under UV (d, middle panel), H_2O_2 as shown by DAB staining (d, right panel) and an increase in the steady state level of hsr203 transcripts as measured by RT-qPCR (e). Fold increase represents the relative level of expression compared to the EGFP-expressing control.

last 50 amino acids were exchanged in two reciprocal recombinant clones. These 50 residues span the PRM2 and C-terminal domain containing divergent amino acids. The recombinant clones were called $2A_{F209G}$:EGFP and $2A_{G209F}$:EGFP, where the first subscript letter indicates the GFLV strain from which the N-terminus originated, the second subscript letter indicates the strain from which the C-terminus originated and 209 gives the position of the first swapped residue (Fig. 4a,c). The EGFP-tagged chimeric proteins exhibited the same cytoplasmic fluorescent aggregates as the parental proteins (Fig. 4c), suggesting that recombination did not substantially disrupt the correct folding of the protein.

The expression of recombinant protein $2A_{G209F}$:EGFP (which contains the 50 C-terminal amino acids of GFLV-F13) induced a necrotic reaction on agroinfiltrated *N. occidentalis* leaves at 5–7 dpi, preceded by the production of phytoalexins and H_2O_2, and an increased accumulation of hsr203J transcripts, similar to $2A_F$:EGFP. By contrast, the expression of recombinant protein $2A_{F209G}$:EGFP caused no symptoms, similar to the $2A_G$:EGFP control (Fig. 4d,e). These results show that the HR-eliciting property of the GFLV-F13 protein $2A^{HP}$ maps to the 50 distal amino acids.

Do the C-terminal 50 amino acids of GFLV-F13 $2A^{HP}$ limit virus propagation?

To test whether the C-terminus of protein $2A^{HP}$ is involved in virus restriction, recombinant $2A^{HP}$ coding sequences were introduced back into the GFLV RNA2 cDNAs to engineer the recombinants F1F2($2A_{F209G}$) and G1G2($2A_{G209F}$). Recombinant F1F2($2A_{F209G}$) reproduced a compatible reaction with no symptoms on inoculated leaves and a mosaic on apical leaves, as observed in plants infected with viral constructs harbouring the GFLV-GHu protein $2A^{HP}$ sequence (Table 1 and Fig. S1a, see Supporting Information). In addition, the virus titre was comparably high to that of inocula encoding the GFLV-GHu protein $2A^{HP}$. Reciprocally, recombinant G1G2($2A_{G209F}$) reproduced the necrotic lesions on inoculated leaves (Fig. S1b) and the virus titre was low (1 μg/g of fresh leaf tissue in inoculated leaves), confirming the results from transient expression experiments (Table 1). The two phenotypes on apical leaves (no symptoms or chlorotic and necrotic spots to leaf deformation) were identical to those observed with other viral constructs carrying the GFLV-F13 protein $2A^{HP}$. Either no virus or less than 1 μg of virus/g of leaf tissue were detected, showing that the C-terminal 50 amino acids of $2A_F$ limit virus propagation, although virus accumulation occurs in uninoculated apical leaves (Table 1). The sequence of the complete genome progeny was verified to correspond to the recombinant inocula. Together, these results show, in both a loss- and gain-of-function approach, that the C-terminal 50 amino acids of GFLV-F13 protein $2A^{HP}$ elicit an HR that limits virus propagation.

DISCUSSION

In this work, we have demonstrated, by reciprocal exchanges made in the infectious clones of two GFLV strains, that protein $2A^{HP}$ of GFLV-F13 determines a strain-specific necrosis on inoculated leaves of the herbaceous host *N. occidentalis*. The accumulation of hallmarks of HR, i.e. phytoalexins, ROS, PR1c and hsr203J transcripts, revealed that the necrotic phenotype fulfils the criteria of a *bona fide* HR. Transient expression of protein $2A^{HP}$ fused to an EGFP tag demonstrated that the protein is sufficient to trigger HR and can therefore be considered as an Avr factor. The use of an untranslatable sequence further showed that the protein, rather than the RNA, elicits an HR. These features are consistent with those of the vast majority of Avr factors described so far (de Ronde *et al.*, 2014), with only very limited examples of avirulent RNAs (Szittya and Burgyán, 2001).

This work, demonstrating the role of $2A^{HP}$ as a viral determinant of symptoms in an incompatible interaction between GFLV and *N. occidentalis*, completes a previous study on other Nicotianae plants, where $1E^{Pol}$ was shown to determine the mosaic symptoms in a compatible reaction (Vigne *et al.*, 2013). This specificity suggests that protein $2A^{HP}$ of GFLV-F13 interacts with a resistance gene product; either directly or via a guard factor, only in this particular *Nicotiana* species, and not in other tested Nicotianae. This hypothesis is corroborated by the absence of necrosis on transient expression of $2A_F$:EGFP or $2A_{G209F}$:EGFP proteins in *N. benthamiana* (this work), and by the similar accumulation of F13 and GHu strains in *N. benthamiana* or *N. clevelandii* (Vigne *et al.*, 2013).

GFLV-F13 protein $2A^{HP}$ is the first Avr factor identified in the genus *Nepovirus* that accounts for HR triggered by a viral infection on a host plant. Transient expression of a portion of the helicase protein of *Tobacco ringspot virus* (TRSV, another subgroup A nepovirus), which encompasses an amphipathic helix, induces cell death in *N. benthamiana* (Hashimoto *et al.*, 2015). However, this necrotic phenotype is not observed in TRSV-infected *N. benthamiana*, a result that questions the link between virus-induced symptoms and the elicitor activity of the amphipathic helix (Hashimoto *et al.*, 2015). Similarly, an RNA structure of *Grapevine chrome mosaic virus* (GCMV) expressed in a viral vector induced necrosis in host and non-host *Nicotiana* species (Fernandez *et al.*, 1999), a phenotype which is not observed in GCMV-infected plants. Such symptoms induced by viral sequences only when expressed outside of the viral context could indicate either an intrinsic property of the RNA sequence, which is counteracted during virus infection, or an interaction with a host factor that does not exist during the infection cycle.

Based on sequence comparisons between nepovirus isolates and the fact that the GFLV $2A^{HP}$ coding sequence seems to be under weaker selection pressure than other coding sequences (Oliver *et al.*, 2010), the N-terminal region of protein $2A^{HP}$ was

predicted as a host or symptom determinant in grapevine (Elbeaino *et al.*, 2014). Here, the GFLV protein $2A^{HP}$ was shown to determine symptomatology on *N. occidentalis*; however, the 50 C-terminal residues cause the necrotic phenotype. Although globally more conserved among nepoviruses, this region contains 17 different residues between GFLV strains F13 and GHu. As it is not uncommon for single amino acids to act as symptom determinants (Divéki *et al.*, 2004; Hasiów-Jaroszewska *et al.*, 2011; Kagiwada *et al.*, 2005; Ozeki *et al.*, 2006), these 17 different residues could be tested individually to identify the minimal number of amino acid(s) involved in the necrotic response of *N. occidentalis* to GFLV-F13 infection. Alternatively, a more complex amino acid pattern could determine symptomatology, as is the case for the tobacco vein necrosis symptoms induced by *Potato virus* Y^N isolates, for which three amino acids scattered throughout the HC-Pro sequence (N_{339}, K_{400} and E_{419}) are important determinants, although they do not alone explain all known relationships between genotype and phenotype (Faurez *et al.*, 2012).

The Avr role of protein $2A^{HP}$ of GFLV-F13 was determined in the context of virus infection by gene exchanges between two GFLV strains, making sure the sequence was in a viral background very similar to that from which it originated (Szittya and Burgyán, 2001). This feature has the advantage of avoiding the use of a vector derived from a heterologous virus, a system which can modify the virulence activity of a viral factor (Li *et al.*, 1999; Szittya and Burgyán, 2001). The Avr nature of protein $2A^{HP}$ of GFLV-F13 was further verified and mapped in a transient expression assay as a C-terminal fusion to EGFP. In the absence of this fusion, no necrosis was observed (data not shown). As an anti-2A serum is unavailable, the expression and stability of protein $2A^{HP}$ could not be analysed. The instability of an unfused protein $2A^{HP}$ has been hypothesized previously to explain the need for non-viral sequences in GFLV RNA2 replication during protoplast transfection (Gaire *et al.*, 1999). The coding sequence of both the $2B^{MP}$ and $2C^{CP}$ products could be deleted without affecting the RNA2 replication, as long as the $2A^{HP}$ sequence was fused to the GFP coding sequence. This was interpreted as a possible need for a protein stabilization role by the downstream heterologous coding sequence, although this hypothesis was not further tested with non-coding sequences. In the context of an HR elicitor, a similar need for protein $2A^{HP}$ stabilization could be critical for a direct or an indirect recognition of the host R protein.

The local HR induced by WT GFLV-F13, synthetic assortant G1F2 and recombinants G1G2($2A_F$) and G1G2($2A_{G209F}$) is insufficient to restrict the virus to the inoculation sites in all inoculated plants. Indeed, only a small proportion of the inoculated plants showed a complete absence of virus accumulation in the uninoculated apical leaves, although necrosis was visible on inoculated leaves (Table 1).

It is probable that viral escape did not result from viral mutations, as indicated by the sequencing of large segments of the progeny genome. Thus, the variability in the level of resistance to GFLV infection most probably reflects the dynamics of virus–plant interaction outcomes, with some plants reacting rapidly and sufficiently strongly to establish an efficient resistance, whereas other plants react slowly or weakly and fight with limited efficacy against the virus (Künstler *et al.*, 2016). Alternatively, the virus could replicate more rapidly in the latter plants and overcome the plant defence. In both cases, a variable physiological state of the plants could explain the differences in the outcome of the competition between plant defence and virus spread. An inefficient systemic resistance following an initial HR-type symptom induction has been described previously in tobacco plants infected with ToRSV, a subgroup C nepovirus, which is partially restricted in only a fraction of plants (Jovel *et al.*, 2011). Thus, nepoviruses belong to an increasing list of viruses for which there is no strict correlation between HR and virus restriction (Bendahmane *et al.*, 1999; Chu *et al.*, 2000; Culver and Dawson, 1989; Sekine *et al.*, 2006).

The mechanism by which the virus is partially restricted in our model plant remains to be explored. Induced cell death and defence reactions by the HR could explain the limited virus multiplication and spread. Alternatively, as protein $2A^{HP}$ is involved in RNA2 replication (Gaire *et al.*, 1999), and thus indirectly in encapsidation and movement, the host resistance gene could act directly by inhibiting virus replication and movement. However, many Avr factors act independently of virus accumulation (Hasiów-Jaroszewska *et al.*, 2011; Mansilla *et al.*, 2009; Schoelz, 2006). Future experiments will aim to uncouple these two functions of GFLV protein $2A^{HP}$.

EXPERIMENTAL PROCEDURES

Virus strains and corresponding infectious cDNA clones

Strains F13 and GHu of GFLV (Ritzenthaler *et al.*, 1991; Serghini *et al.*, 1990; Vigne *et al.*, 2008) were propagated on *Chenopodium quinoa*. Full-length cDNA clones corresponding to all genomic RNAs under the control of the T7 transcription promoter were available at the onset of this study for the *in vitro* synthesis of infectious transcripts (Vigne *et al.*, 2013; Viry *et al.*, 1993). Transcripts F1, F2, G1 and G2 correspond to RNA1 of GFLV-F13, RNA2 of GFLV-F13, RNA1 of GFLV-GHu and RNA2 of GFLV-GHu, respectively.

Development of chimeric GFLV-F13 and GFLV-GHu RNA2

PCRs for cloning purposes were carried out using the Phusion polymerase (Finnzyme, Vantaa, Finland). Plasmid pGORF2 (Vigne *et al.*, 2013) containing the P2 coding sequence of GFLV-GHu and the 5′ and 3′ UTRs of GFLV-F13 (Fig. S2b, see Supporting Information) was digested with *Alw*NI and *Age*I. The 1815-nucleotide-long fragment was cloned into plasmid pF2 after *Alw*NI/*Age*I digestion. The resulting pF2($2A_G$) plasmid contains the

$2A^{HP}$ coding sequence of GFLV-GHu in a GFLV-F13 backbone. As a result of the use of a restriction site within the $2B^{MP}$ coding sequence, pF2($2A_G$) also encodes an arginine (Arg) residue of GHu origin at the fourth position of the $2B^{MP}$ coding region (Fig. S2c). The reciprocal plasmid pG2($2A_F$) was obtained by overlap PCR extension (Ho *et al.*, 1989). The GFLV-F13 $2A^{HP}$ coding sequence was PCR amplified with primers G80 and G79, whereas the GFLV-GHu RNA2-5′UTR was PCR amplified with primers G78 and G82 (Table S1, see Supporting Information). These overlapping fragments were assembled by PCR amplification using primers G78 and G79, and the amplicon was inserted into an *Alw*NI/*Age*I-digested plasmid pG2 to give rise to plasmid pG2($2A_F$). It is noteworthy that this recombinant plasmid also codes for a lysine (Lys) residue of F13 origin at the fourth position of the GHu-$2B^{MP}$ sequence (Fig. S2c).

Plasmids pG2($2A_{G209F}$) and pF2($2A_{G209F}$), allowing the transcription of the recombinant RNAs G2($2A_{G209F}$) and F2($2A_{F209G}$), were assembled from plasmids pG2 and pF2 by replacing the *Rsr*II/*Age*I restriction fragments by the corresponding fragments amplified from pK7FWG2-$2A_{G209F}$ and pK7FWG2-$2A_{F209G}$ (see 'Transient expression of WT and mutant $2A^{HP}$ proteins' section) with primers E28 and E46, and primers E28 and E45, respectively.

All plasmids were amplified in *Escherichia coli* and checked by enzyme restriction and sequencing (primers in Table S2, see Supporting Information).

In vitro transcription of viral cDNA clones and mechanical inoculation

Transcripts were synthesized by *in vitro* transcription of the corresponding linearized plasmids using the mMESSAGE mMACHINE T7 kit (Ambion, Foster City, California, USA). *C. quinoa* plants (four- to six-leaf stage) were mechanically inoculated by rubbing the leaf blades with transcripts corresponding to WT or recombinant GFLV-RNA1 and GFLV-RNA2, or combinations thereof. Symptoms were monitored at 6–14 dpi and systemic infection was assessed in uninoculated apical leaves at 14 dpi by DAS-ELISA (Vigne *et al.*, 2013). *N. occidentalis* plants (four- to six-leaf stage) were mechanically inoculated with the crude sap of infected *C. quinoa* after estimating the virus titre by semi-quantitative DAS-ELISA and adjusting the inoculum to 350 ng per plant (corresponding to crude sap of 1.2–3.5 g of infected *C. quinoa* leaf tissue). Symptoms were monitored for at least 14 dpi and virus accumulation in inoculated and uninoculated leaves was estimated by semi-quantitative DAS-ELISA at 10 dpi. These inoculation experiments were repeated at least twice with passages or purified viruses.

Sequencing of GFLV progeny

The progeny of WT (F13 and GHu), synthetic (F1F2 and G1G2), assorted (F1G2 and G1F2) and chimeric (F1F2-$2A_G$, G1G2-$2A_F$, F1F2-$2A_{F209G}$ and G1G2-$2A_{G209F}$) viruses were characterized at 10 dpi by IC-RT-PCR (Vigne *et al.*, 2004). The RT reaction was primed using oligo(dT) or random primers. PCR was performed with specific primer pairs, generating eight and five overlapping fragments for RNA1 and RNA2, respectively. Sequencing covered almost the complete RNA1 (nucleotides 160–7270) and RNA2 (nucleotides 60–3780) for recombinants F1F2-$2A_{F209G}$ and G1G2-$2A_{G209F}$, and from the end of the $1E^{Pol}$ coding sequence to the 3′ UTR end of RNA1 (nucleotides 6530–7270) and from the end of the $2A^{HP}$ coding sequence into the $2B^{MP}$ coding sequence of RNA2 (nucleotides 800–1500) for all the other virus constructs. The primers used for sequencing are listed in Table S2.

Detection of GFLV by DAS-ELISA and semi-quantitative DAS-ELISA

GFLV detection by DAS-ELISA and virus titre determination in *N. occidentalis* by semi-quantitative DAS-ELISA were performed as described previously (Vigne *et al.*, 2013). The virus concentration in the crude sap of *C. quinoa* was estimated for inoculum calibration in a rapid (1-day) semi-quantitative DAS-ELISA by reducing the incubation times (Table S4, see Supporting Information) to allow for same-day inoculations.

Transient expression of WT and mutant $2A^{HP}$ proteins

Gateway technology (Invitrogen, Carlsbad, California, USA) was used to construct plasmids for transient expression. The GFLV-F13 and GFLV-GHu $2A^{HP}$ coding region was PCR amplified and flanked with attB1 and attB2 recombination sequences, from pF2 and pG2, using primers m36 and m44, and primers 104 and 105, respectively (Table S1). After a first recombination into the donor plasmid pDONR/Zeo, the $2A^{HP}$ coding sequences were further recombined into the destination vector pK7FWG2 (Karimi *et al.*, 2002).

To transiently express recombinant proteins $2A_{F209G}$ and $2A_{G209F}$, plasmids pK7FWG2-$2A_{F209G}$ and pK7FWG2-$2A_{G209F}$ were constructed with overlap PCR extension (Fig. S3a, see Supporting Information). For pK7FWG2-$2A_{F209G}$, an N-proximal fragment was amplified using pF2 as a template and primers E31 and E34, whereas the C-terminal fragment was amplified from plasmid pG2 with primers E33 and E29 (Table S1). The amplicons were assembled and flanking attB1 and attB2 sequences were added during a third amplification PCR with primers m36 and 105. The resulting fragment was successively recombined into pDonR/Zeo and pK7FWG2 Gateway vectors. The reciprocal pK7FWG2-$2A_{G209F}$ was similarly obtained from plasmid pG2 with primers E30 and E34, and plasmid pF2 with primers E33 and E32 (Table S1). The fragments were assembled together and flanked with attB sequences with primers 104 and m44 prior to recombination into pDonR/Zeo and pK7FWG2 vectors.

As a result of the Gateway cassette in the pK7FWG2 vector, a non-recombined vector does not correspond to a classical empty control vector and, consequently, would not allow expression of the EGFP tag. Thus, we recombined the pDonR/Zeo vector with a DNA fragment (amplified from the TagRFP sequence with primers 511 and 512) flanked by two *Avr*II restriction sites, one immediately downstream of the attB1 sequence and the second, together with an initiation codon, immediately upstream of the attB2 sequence. The removal of the *Avr*II restriction fragment from the entry clone prior to recombination into pK7FWG2 resulted in plasmid pK7FWG2-Control, which only differs from the pK7FWG2-2A constructs by an extra *Avr*II site and the absence of any $2A^{HP}$ coding sequence (Fig. S3b). This plasmid allows the expression of an untagged EGFP.

Plasmid pK7FWG2-$2A_{F\text{-}Stop}$, which allows the transcription of an untranslatable RNA, was obtained by recombination of the destination vector with a mutagenized entry vector. Mutagenesis was performed using the Quick Change II kit (Stratagene, San Diego – La Jolla, California,

USA), the reverse primer m44 and the mutagenic forward primer IM11, in which (i) the start codon ATG is changed into TTG and (ii) the fifth sense codon (TAT) is changed into a stop codon (TAA).

Deletion mutants within protein $2A^{HP}$ were constructed as follows: (i) by PCR using primers m37, m38, m44, m43 and m36 containing attB1 or attB2 recombination sequences fused to the target border sequence, for the N- and C-terminal deletions ΔN40, ΔN82 and ΔC43, and subsequent recombination into the pDonR/Zeo donor plasmid; (ii) by inverse PCR on the pDonR/Zeo-$2A_F$ plasmid using the Quick Change kit and the mutagenic primers m39 with m40 and m41 with m42 for internal deletions ΔPRM1 and ΔPRM2; and (iii) by restriction digestion of the pDonR/Zeo-$2A_F$ plasmid with *Eco*NI, Klenow filling and ligation for ΔM75. All the mutant constructs were sequenced, recombined into the pK7FWG2 destination vector and further checked by restriction digestion and sequencing, before transformation of *Agrobacterium tumefaciens* strain GV3101::pMP90 (Koncz *et al.*, 1994) by heat shock (Sparkes *et al.*, 2006) or electroporation. For protein expression, freshly transformed or streaked agrobacteria were grown overnight at 28 °C, centrifuged, washed and resuspended in 10 mM 2-(N-morpholino)ethanesulfonic acid(MES), pH 5.7, 10 mM $MgCl_2$ at an optical density at 600 nm (OD_{600}) of 0.4–0.5 prior to plant infiltration. To optimize protein expression, agrobacteria with a binary plasmid encoding the *tomato bushy stunt virus* suppressor of silencing P19 were co-infiltrated at a 1 : 1 ratio in all samples, including the EGFP-expressing control. The transient expression of recombinant 2A proteins fused to EGFP was conducted at least four times on four to nine plants.

Protein extraction and western blot analysis

For the detection of PR1c, total proteins were extracted from agroinfiltrated leaf patches (2–5 dpi) or inoculated leaves (8–10 dpi) of *N. occidentalis* in phosphate-buffered saline, pH 7.4, in the presence of protease inhibitors (Complete, Roche, Basel, Switzerland). For the detection of protein 2A:EGFP, proteins were extracted with phenol and precipitated with ammonium acetate in methanol (Hurkman and Tanaka, 1986). In both cases, proteins were resolved by electrophoresis in sodium dodecylsulfate-polyacrylamide gels and electrotransferred onto Immobilon Polyvinylene fluoride (PVDF) membranes. Specific polyclonal PR1c and GFP antisera, kindly provided by T. Heitz (Heitz *et al.*, 1994) and D. Scheidecker, were used in western blot analysis at 1 : 5000 and 1 : 10 000 dilutions, respectively. Horseradish peroxidase-conjugated goat anti-rabbit antibodies (1 : 12 500) and the lumi-light chemiluminescence system (Roche) were used for antigen detection. Loading was controlled by Coomassie blue staining.

Gene expression analysis by quantitative RT-PCR

Total RNA was extracted from 50 mg of *N. occidentalis* leaf tissue using the RNeasy Plant Mini Kit (Qiagen, Hilden, Germany). After DNase treatment, 1 μg of total RNA was reverse transcribed in 20 μL using the SuperScript II Reverse Transcriptase (Invitrogen, Carlsbad, CA, USA) and oligo(dT) primers. Quantitative PCRs were performed in a CFX96 system (Bio-Rad, Hercules, CA, USA) using SsoFast™EvaGreen®Supermix. Thermal cycling conditions were 30 s at 95 °C, followed by 40 cycles of 5 s at 95 °C, 5 s at 55 °C and 30 s at 72 °C. The results were normalized to the expression of three reference genes, Actin (GenBank JQ256516.1), Cdc2 (GenBank D50738.1) and EF1α (GenBank AY206004.1), as described previously (Vandesompele *et al.*, 2002). The relative expression (fold induction) compared with appropriate controls (mock-inoculated leaves for the infection experiments and EGFP-expressing leaf patches for the transient expression experiments) was calculated with the Livak method ($\Delta\Delta Ct$) after primer efficiencies had been checked. Mean values and standard deviations were obtained from at least three technical and two biological replicates. The primers used are listed in Table S3 (see Supporting Information).

Plant growth conditions

N. occidentalis, *N. benthamiana* and *C. quinoa* plants were grown in a glasshouse at 22 °C (with fluctuations from 18 to 26 °C) with a 14-h/10-h (light/dark) photoperiod. Agroinfiltrated plants were transferred to a growth chamber with an 18 °C/22 °C (day/night) temperature regime and a 14-h/10-h (light/dark) photoperiod.

DAB staining

Staining of entire leaves or leaf discs with DAB was performed as described previously (Daudi and O'Brien, 2012).

ACKNOWLEDGEMENTS

We thank Lalaina Rakotomalala and Shahinez Garcia for technical assistance, Drs Jean-Michel Hily and Julie Chong for helpful discussions, and Dr Thierry Heitz and Danièle Scheidecker for the generous gift of anti-PR1c and anti-GFP sera, respectively. This work was supported in part by INRA and by a fellowship from Moët & Chandon, Comité Interprofessionnel du Vin de Champagne, Bureau Interprofessionnel des Vins de Bourgogne and the Conseil Interprofessionnel des Vins d'Alsace to I.R.M.

REFERENCES

Andret-Link, P., Laporte, C., Valat, L., Ritzenthaler, C., Demangeat, G., Vigne, E., Laval, V., Pfeiffer, P. and Fuchs, M. (2004) *Grapevine fanleaf virus*: still a major threat to the grapevine industry. *J. Plant Pathol.* **86**, 183–195.

Bendahmane, A., Kanyuka, K. and Baulcombe, D.C. (1999) The Rx gene from potato controls separate virus resistance and cell death responses. *Plant Cell*, **11**, 781–791.

Chong, J., Baltz, R., Schmitt, C., Beffa, R., Fritig, B. and Saindrenan, P. (2002) Downregulation of a pathogen-responsive tobacco UDP-Glc:phenylpropanoid glucosyltransferase reduces scopoletin glucoside accumulation, enhances oxidative stress, and weakens virus resistance. *Plant Cell*, **14**, 1093–1107.

Chu, M., Desvoyes, B., Turina, M., Noad, R. and Scholthof, H.B. (2000) Genetic dissection of tomato bushy stunt virus P19-protein-mediated host-dependent symptom induction and systemic invasion. *Virology*, **266**, 79–87.

Cornelissen, B.J.C., van Huijsduijnen, R.A.M.H., Van Loon, L.C. and Bol, J.F. (1986) Molecular characterization of messenger RNAs for 'pathogenesis-related' proteins 1a, 1b and 1c, induced by TMV infection of tobacco. *EMBO J.* **5**, 37–40.

Culver, J.N. and Dawson, W.O. (1989) Point mutations in the coat protein gene of tobacco mosaic virus induce hypersensitivity in *Nicotiana sylvestris*. *Mol. Plant–Microbe Interact.* **2**, 209–213.

Dangl, J.L. and Jones, J.D.G. (2001) Plant pathogens and integrated defence responses to infection. *Nature*, **411**, 826–833.

Daudi, A. and O'Brien, J.A. (2012) Detection of hydrogen peroxide by DAB staining in Arabidopsis leaves. *Bio Protoc.* **2**, e263.

Dinesh-Kumar, S.P., Tham, W.-H. and Baker, B.J. (2000) Structure–function analysis of the tobacco mosaic virus resistance gene *N*. *Proc. Natl. Acad. Sci. USA*, **97**, 14 789–14 794.

Divéki, Z., Salánki, K. and Balázs, E. (2004) The necrotic pathotype of the cucumber mosaic virus (CMV) Ns strain is solely determined by amino acid 461 of the 1a protein. *Mol. Plant–Microbe Interact.* **17**, 837–845.

Elbeaino, T., Kiyi, H., Boutarfa, R., Minafra, A., Martelli, G. and Digiaro, M. (2014) Phylogenetic and recombination analysis of the homing protein domain of grapevine fanleaf virus (GFLV) isolates associated with 'yellow mosaic' and 'infectious malformation' syndromes in grapevine. *Arch. Virol.* **159**, 2757–2764.

Faurez, F., Baldwin, T., Tribodet, M. and Jacquot, E. (2012) Identification of new *Potato virus Y* (PVY) molecular determinants for the induction of vein necrosis in tobacco. *Mol. Plant Pathol.* **13**, 948–959.

Fernandez, I., Candresse, T., Le Gall, O. and Dunez, J. (1999) The 5′ noncoding region of grapevine chrome mosaic nepovirus RNA-2 triggers a necrotic response on three *Nicotiana* spp. *Mol. Plant–Microbe Interact.* **12**, 337–344.

Fuchs, M., Schmitt-Keichinger, C. and Sanfaçon, H. (2017) A renaissance in nepovirus research provides new insights into their molecular interface with hosts and vectors. *Adv Virus Res.* **97**, 61–105.

Gaire, F., Schmitt, C., Stussi-Garaud, C., Pinck, L. and Ritzenthaler, C. (1999) Protein 2A of Grapevine fanleaf nepovirus is implicated in RNA2 replication and colocalizes to the replication site. *Virology*, **264**, 25–36.

Ghoshal, B. and Sanfaçon, H. (2015) Symptom recovery in virus-infected plants: revisiting the role of RNA silencing mechanisms. *Virology*, **479–480**, 167–179.

Hashimoto, M., Komatsu, K., Iwai, R., Keima, T., Maejima, K., Shiraishi, T., Ishikawa, K., Yoshida, T., Kitazawa, Y., Okano, Y., Yamaji, Y. and Namba, S. (2015) Cell death triggered by a putative amphipathic helix of radish mosaic virus helicase protein is tightly correlated with host membrane modification. *Mol. Plant–Microbe Interact.* **28**, 675–688.

Hasiów-Jaroszewska, B., Borodynko, N., Jackowiak, P., Figlerowicz, M. and Pospieszny, H. (2011) Single mutation converts mild pathotype of the Pepino mosaic virus into necrotic one. *Virus Res.* **159**, 57–61.

Heitz, T., Fritig, B. and Legrand, M. (1994) Local and systemic accumulation of PR proteins in tobacco plants infected with *Tobacco mosaic virus*. *Mol. Plant–Microbe Interact.* **7**, 776–779.

Ho, S.N., Hunt, H.D., Horton, R.M., Pullen, J.K. and Pease, L.R. (1989) Site-directed mutagenesis by overlap extension using the polymerase chain reaction. *Gene*, **77**, 51–59.

Hurkman, W. and Tanaka, C. (1986) Solubilization of plant membrane proteins for analysis by two-dimensional gel electrophoresis. *Plant Physiol.* **81**, 802–806.

Jovel, J., Walker, M. and Sanfaçon, H. (2007) Recovery of *Nicotiana benthamiana* plants from a necrotic response induced by a nepovirus is associated with RNA silencing but not with reduced virus titer. *J. Virol.* **81**, 12 285–12 297.

Jovel, J., Walker, M. and Sanfaçon, H. (2011) Salicylic acid-dependent restriction of *Tomato ringspot virus* spread in tobacco is accompanied by a hypersensitive response, local RNA silencing, and moderate systemic resistance. *Mol. Plant–Microbe Interact.* **24**, 706–718.

Kagiwada, S., Yamaji, Y., Komatsu, K., Takahashi, S., Mori, T., Hirata, H., Suzuki, M., Ugaki, M. and Namba, S. (2005) A single amino acid residue of RNA-dependent RNA polymerase in the Potato virus X genome determines the symptoms in *Nicotiana* plants. *Virus Res.* **110**, 177–182.

Karimi, M., Inzé, D. and Depicker, A. (2002) GATEWAY™ vectors for Agrobacterium-mediated plant transformation. *Trends Plant Sci.* **7**, 193–195.

Koncz, C., Martini, N., Szabados, L., Hrouda, M., Bachmair, A. and Schell, J. (1994) Specialized vectors for gene tagging and expression studies. In: *Plant Molecular Biology Manual* (Gelvin, S. and Schilperoort, B., eds.), pp. 1–22. Dordrecht: Kluwer Academic.

Künstler, A., Bacsó, R., Gullner, G., Hafez, Y.M. and Király, L. (2016) Staying alive – is cell death dispensable for plant disease resistance during the hypersensitive response?. *Physiol. Mol. Plant Pathol.* **93**, 75–84.

Lamb, C. and Dixon, R.A. (1997) The oxidative burst in plant disease resistance. *Annu. Rev. Plant Phys.* **48**, 251–275.

Li, H.W., Lucy, A.P., Guo, H.S., Li, W.X., Ji, L.H., Wong, S.M. and Ding, S.W. (1999) Strong host resistance targeted against a viral suppressor of the plant gene silencing defence mechanism. *EMBO J.* **18**, 2683–2691.

Mansilla, C., Sánchez, F., Padgett, H.S., Pogue, G.P. and Ponz, F. (2009) Chimeras between *Oilseed rape mosaic virus* and *Tobacco mosaic virus* highlight the relevant role of the tobamoviral RdRp as pathogenicity determinant in several hosts. *Mol. Plant Pathol.* **10**, 59–68.

Oliver, J.E., Vigne, E. and Fuchs, M. (2010) Genetic structure and molecular variability of Grapevine fanleaf virus populations. *Virus Res.* **152**, 30–40.

Ozeki, J., Takahashi, S., Komatsu, K., Kagiwada, S., Yamashita, K., Mori, T., Hirata, H., Yamaji, Y., Ugaki, M. and Namba, S. (2006) A single amino acid in the RNA-dependent RNA polymerase of Plantago asiatica mosaic virus contributes to systemic necrosis. *Arch. Virol.* **151**, 2067–2075.

Palukaitis, P. (2011) The road to RNA silencing is paved with plant–virus interactions. *Plant Pathol. J.* **27**, 197–206.

Pontier, D., Godiard, L., Marco, Y. and Roby, D. (1994) hsr203J, a tobacco gene whose activation is rapid, highly localized and specific for incompatible plant/pathogen interactions. *Plant J.* **5**, 507–521.

Pontier, D., Tronchet, M., Rogowsky, P., Lam, E. and Roby, D. (1998) Activation of hsr203, a plant gene expressed during incompatible plant–pathogen interactions, is correlated with programmed cell death. *Mol. Plant–Microbe Interact.* **11**, 544–554.

Ritzenthaler, C., Viry, M., Pinck, M., Margis, R., Fuchs, M. and Pinck, L. (1991) Complete nucleotide sequence and genetic organization of grapevine fanleaf nepovirus RNA1. *J. Gen. Virol.* **72**, 2357–2365.

de Ronde, D., Butterbach, P. and Kormelink, R. (2014) Dominant resistance against plant viruses. *Front. Plant Sci.* **5**, 307–323.

Sanfaçon, H. (2008) Nepovirus. In: *Encyclopedia of Virology, 3rd edn.* (Mahy, B.W.J. and van Regenmortel, M.H.V., eds.), pp. 405–413. Oxford: Academic Press.

Schoelz, J.E. (2006) Viral determinants of resistance versus susceptibility. In: *Natural Resistance Mechanisms of Plants to Viruses* (Loebenstein, G. and Carr, J.P., eds.), pp. 13–43. Dordrecht: Springer.

Scholthof, K.-B.G. (2008) Tobacco mosaic virus: the beginning of plant pathology. *Online. APSnet Features*. doi: 10.1094/APSnetFeatures-2008-0408

Sekine, K.-T., Ishihara, T., Hase, S., Kusano, T., Shah, J. and Takahashi, H. (2006) Single amino acid alterations in *Arabidopsis thaliana* RCY1 compromise resistance to cucumber mosaic virus, but differentially suppress hypersensitive response-like cell death. *Plant Mol. Biol.* **62**, 669–682.

Sels, J., Mathys, J., De Coninck, B.M.A., Cammue, B.P.A. and De Bolle, M.F.C. (2008) Plant pathogenesis-related (PR) proteins: a focus on PR peptides. *Plant Physiol. Biochem.* **46**, 941–950.

Serghini, M.A., Fuchs, M., Pinck, M., Reinbolt, J., Walter, B. and Pinck, L. (1990) RNA2 of Grapevine fanleaf virus: sequence analysis and coat protein cistron location. *J. Gen. Virol.* **71**, 1433–1441.

Sparkes, I.A., Runions, J., Kearns, A. and Hawes, C. (2006) Rapid, transient expression of fluorescent fusion proteins in tobacco plants and generation of stably transformed plants. *Nat. Protoc.* **1**, 2019–2015.

Szittya, G. and Burgyán, J. (2001) Cymbidium ringspot tombusvirus coat protein coding sequence acts as an avirulent RNA. *J. Virol.* **75**, 2411–2420.

Thordal-Christensen, H., Zhang, Z., Wei, Y. and Collinge, D.B. (1997) Subcellular localization of H_2O_2 in plants. H_2O_2 accumulation in papillae and hypersensitive response during the barley—powdery mildew interaction. *Plant J.* **11**, 1187–1194.

Vandesompele, J., De Preter, K., Pattyn, F., Poppe, B., Van Roy, N., De Paepe, A. and Speleman, F. (2002) Accurate normalization of real-time quantitative RT-PCR data by geometric averaging of multiple internal control genes. *Genome Biol.* **3**, research0034.

Vigne, E., Bergdoll, M., Guyader, S. and Fuchs, M. (2004) Population structure and genetic variability within isolates of *Grapevine fanleaf virus* from a naturally infected vineyard in France: evidence for mixed infection and recombination. *J. Gen. Virol.* **85**, 2435–2445.

Vigne, E., Marmonier, A. and Fuchs, M. (2008) Multiple interspecies recombination events within RNA2 of *Grapevine fanleaf virus* and *Arabis mosaic virus*. *Arch. Virol.* **153**, 1771–1776.

Vigne, E., Gottula, J., Schmitt-Keichinger, C., Komar, V., Ackerer, L., Belval, L., Rakotomalala, L., Lemaire, O., Ritzenthaler, C. and Fuchs, M. (2013) A strain-specific segment of the RNA-dependent RNA polymerase of *Grapevine fanleaf virus* determines symptoms in *Nicotiana* species. *J. Gen. Virol.* **94**, 2803–2813.

Viry, M., Serghini, M.A., Hans, F., Ritzenthaler, C., Pinck, M. and Pinck, L. (1993) Biologically active transcripts from cloned cDNA of genomic grapevine fanleaf nepovirus RNAs. *J. Gen. Virol.* **74**, 169–174.

Watanabe, N. and Lam, E. (2006) The hypersensitive response in plant disease resistance. In: *Multigenic and Induced Systemic Resistance in Plants* (Tuzun, S. and Bent, E., eds.), pp. 83–111. Boston, MA: Springer.

SUPPORTING INFORMATION

Additional Supporting Information may be found in the online version of this article at the publisher's website:

Table S1 Primers used for cloning.

Table S2 Consensus or degenerate primers used to sequence virus progeny.

Table S3 Primers used for quantitative reverse transcription-polymerase chain reaction (RT-PCR).

Table S4 Comparison of incubation conditions in classical and rapid semi-quantitative double antibody sandwich-enzyme-linked immunosorbent assay (DAS-ELISA).

Fig. S1 Symptoms induced by the recombinant viruses on *Nicotiana occidentalis* inoculated leaves. (a) Symptomless leaf inoculated with F1F2($2A_{F209G}$). Note that some mechanical lesions caused by the inoculation procedure are visible. (b) Intense necrotic lesions on a leaf inoculated with G1G2($2A_{G209F}$).

Fig. S2 Schematic representation of the plasmids used to generate the chimeric F13/GHu RNA2. (a) Genomic organization of RNA2 of GFLV-F13 and GFLV-GHu. The black circle represents the genome-linked VPg and AAAA symbolizes the polyA tail. Narrow open boxes designate 5′ and 3′ untranslated regions (UTRs) and large open boxes represent coding sequences. Grey indicates F13 sequences and white denotes GHu sequences. (b) Infectious cDNA clones available from previous studies. The positions of the three restriction sites used to generate recombinant clones are shown. Note that the *Age*I site lies within the $2B^{MP}$ coding sequence, which only differs by one amino acid sequence upstream of this site between F13 and GHu (K in F13-$2B^{MP}$ vs. R in GHu-$2B^{MP}$). (c) Recombinant clones generated in the present study by swapping either the complete $2A^{HP}$ coding sequence or its 150 3′-terminal nucleotides. The thin line depicts plasmid sequences and the black arrow shows the T7 bacteriophage transcription promoter. Extraviral nucleotides at the junction of the open reading frame (ORF) and the UTRs (narrow open boxes) are indicated.

Fig. S3 Construction of binary vectors for the transient expression of the enhanced green fluorescent protein (EGFP)-tagged wild-type and recombinant proteins $2A_F$:EGFP, $2A_G$:EGFP, $2A_{G209F}$:EGFP and $2A_{F209G}$:EGFP (a) or of the control EGFP (b). Horizontal arrows represent primers. Primers adding attB sequences have double lines and are drawn above the coding regions to which they hybridize. Narrow open boxes represent polymerase chain reaction (PCR) products, whereas wide open boxes represent open reading frames (ORFs) contained in plasmids. Grey filled boxes are of F13 origin, whereas sequences of GHu origin are white. Conserved sequences between *Grapevine fanleaf virus* (GFLV) strains GHu and F13 in which fragments overlap are shaded white to grey. attB sequences are hatched. Light lines represent plasmid sequences. T7 denotes the bacteriophage T7 *in vitro* transcription promoter and 35S is the 35S transcription sequence derived from *Cauliflower mosaic virus*.